

Investigation of Pre-Injection Flow Characteristics in Constant Volume Combustion Chamber (CVCC) using Computational Fluid Dynamics (CFD)

Veeraphol Wang¹, Abhishek Jadav^{1,2}, Ronnachart Munsin¹, Yossapong Laonoual^{1*}

¹ Combustion and Engines Research Laboratory (CERL), Department of Mechanical Engineering, Faculty of Engineering, King Mongkut's University of Technology Thonburi, 126 Pracha Uthit Road, Bang Mod, Thung Kru, Bangkok, 10140, Thailand

² Internship Student, Department of Mechanical Engineering, Indian Institute of Technology, Kanpur, India 208016

* Corresponding Author: E-mail: yossapong.lao@kmutt.ac.th, +66 2470 9123; Fax: +66 2470 9111

Abstract

The present work focuses on the progress of development of a constant volume combustion chamber (CVCC). The objective is to simulate the pre-injection gaseous fluid flow characteristics for four different angles of injection to understand the mixture homogeneity inside the combustion chamber. A 3-D computational fluid dynamics (CFD) software AVL FIRE[®] is used to perform the numerical simulation using finite volume method. Grid independent analysis has been made to optimize CFD process. Two different turbulence models, k- ϵ and k- ζ -f model have been used for the simulation. The results i.e. total pressure, velocity profile and turbulent kinetic energy of both models are compared and analysed at different conditions and are observed to be in agreement with each other. The CVCC with tangential injection is observed to be better than other angle of injection due to homogeneous gaseous mixture.

Keywords: Constant volume combustion chamber (CVCC), CFD, AVL FIRE[®], Turbulence models

1. Introduction

Major factors in the development of modern diesel engines are concern for environment, oil crisis and engine efficiency. To realize this, a variety of technological pathways are being investigated. One of the feasible ways to achieve these is using the bio-fuel [1]. However, it is necessary to study the effect of bio-fuels in order to understand the fundamental of spray and combustion characteristics. For these study, a variety of optical test rigs have been used such as optical research engines (ORE), a rapid compression and expansion machine (RCM), constant pressure flow rigs (CPFR), and constant volume combustion chambers (CVCC). Among

these, CVCC gives a very wide range of gas pressures and temperatures prior to injection with minimal quantities of test fuels [2].

A lean premixed combustible gaseous mixture of fuel (C₂H₂) and synthetic air (O₂ and N₂) is filled into the CVCC (called pre-injection). A spark plug ignites the gaseous mixture and it undergoes combustion reaction (called pre-combustion), which leads to steep pressure and temperature rise. The products of pre-combustion consist of 21% oxygen by volume with complete combustion. Test fuel is then injected by the injector when pressure drops to the target value due to the heat loss to the wall and combustion takes place [3] as shown in Fig. 1.

AEC035

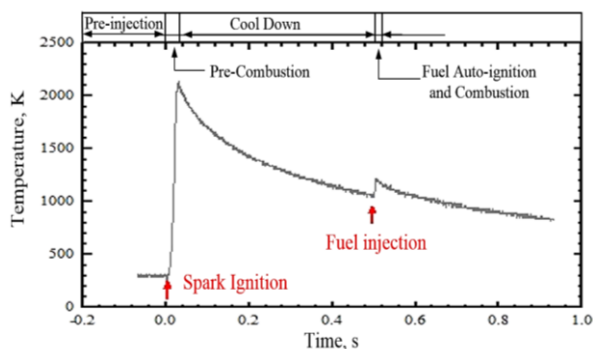


Fig. 1. Principle of pre-combustion technique.

The present work focuses on the detailed understanding of the pre-injection gaseous fluid flow inside CVCC. However, fluid flow in a CVCC is one of the most challenging fluid dynamics problems. It is because the flow inside CVCC is compressible, turbulent, unsteady, cyclic and non-stationary both spatially and temporally [4]. The combustion reaction inside CVCC is greatly influenced by the homogeneity of mixture of fuel and synthetic air, which is mainly controlled by the pre-injection fluid flow. The high turbulent kinetic energy level leads to enhanced fuel and air mixing [5]. So, a detailed understanding of pre-injection gaseous fluid flow in CVCC is required to determine the homogeneity of mixture which leads to the complete combustion.

2. Computational Fluid Dynamics Equations

2.1 Governing Equations

Calculation of the flow field in a constant volume combustion chamber requires obtaining the solution of the governing equations. Compressible, unsteady and turbulent in-cylinder flow can be described by differential equations of continuity, momentum, energy, turbulence kinetic energy and its dissipation rate. The mass conservation and momentum equation are shown in Eq. A.1 and A.2, respectively (in appendix A).

2.2 Turbulence Modelling

In AVL FIRE[®], for turbulent conditions fluctuating parameters are averaged using the Reynolds Averaged Navier-Stokes (RANS) method. There are several turbulence models available, but here k - ζ - f and k - ϵ have been used in these simulation. The standard k - ϵ model equations are shown in the Eq. A.3 - A.7 (appendix B) and the equations for k - ζ - f model are shown in the Eq. A.8 – A.15 (appendix C).

3. CVCC Geometry and 3D Model

Fig. 2 shows the three dimensional model of constant volume combustion chamber. It is cylindrical shape with diameter 100 mm, width 45 mm and volume 350 cm³. In order to understand the mixture homogeneity inside the constant volume combustion chamber, CFD simulation of the pre-injection gaseous fluid flow has been performed for four different angles of injection i.e. 45^o, 75^o, 90^o and tangential to the chamber as shown in Fig. 3. The mesh for case of tangential injection is shown in Fig. 4.

4. Simulation Method

The simulations are done using the AVL Fire code – the CFD software based on the Finite Volume approach dedicated to engine simulation. In this simulation compressible air has been

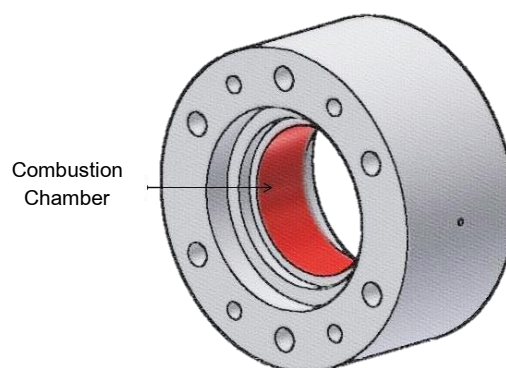


Fig. 2. Model of CVCC for CFD Simulation.

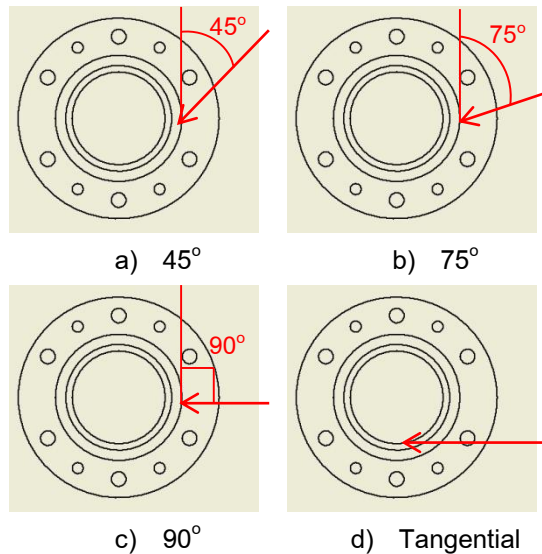


Fig. 3. Angle of injection.

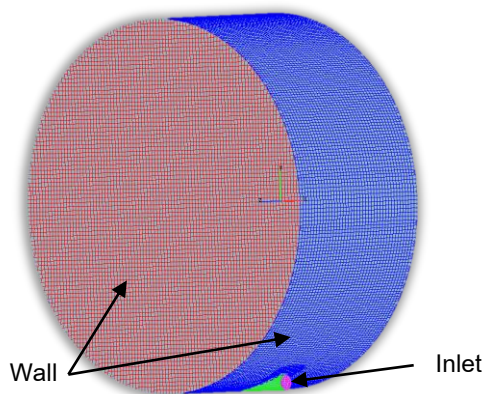


Fig. 4. Mesh for CVCC with tangential inlet.

assumed for the pre-injection gaseous working fluid for CVCC. The fluid flow is considered to be transient. No slip boundary conditions were applied at all walls for all the models. The initial conditions and boundary conditions are listed in Table 2 and Table 3 respectively.

The flow characteristics inside the CVCC are considered as three dimensional. The CFD code uses the SIMPLE algorithm of Patankar [6]. The central differencing scheme is used to discretize the momentum and continuity equations while first order upwind difference scheme (UDS) is used to discretize turbulence equations.

Table 2 Initial Conditions

Pressure	1 bar
Air Density	1.19 kg/m ³
Wall and Air Temperature	20°C
Turbulent Kinetic Energy	1 m ² /s ²
Turbulent Dissipation Rate	1 m ² /s ³

Table 3 Boundary Conditions

Inlet Pressure	10 bar
Wall and Inlet Air Temperature	20°C
Turbulent Kinetic Energy	1 m ² /s ²
Turbulent Dissipation Rate	1 m ² /s ³

5. Results and Discussion

5.1 Grid Independent Analysis

Grid independent study has been done for all models with different injection angle. In order to ensure grid independence and improved accuracy of the results, nine calculations have been done for nine different meshes with different number of cells in each case. In Fig. 5, mean average pressure inside the CVCC for the case with tangential injection angle has been compared with the number of cells in the mesh of the model at three different times i.e. 0.1s, 0.3s and 0.5 s after the start of injection. The appropriate number of cells used in this model is 288,700 as observed from Fig.5.

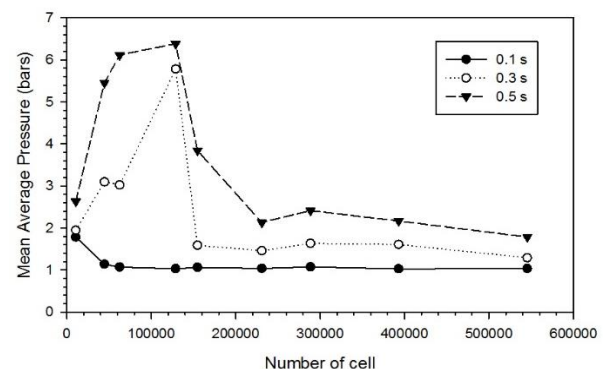


Fig. 5 Grid independent study for the mean average pressure inside CVCC.

AEC035

5.2 Discussion

The results from the numerical simulation are shown in Figs. 6-8. In Fig. 6, the total pressure distribution inside the CVCC has been compared for four different angles of injection between two different turbulence models at time 0.1 seconds after the start of injection. It can be seen that the total pressure at the inlet is close to 10 bar and inside the chamber it is close to 1 bar which is in agreement with the initial and inlet conditions. As the gas is injected inside the chamber the pressure inside starts rising from 1 bar.

Similarly in Fig. 7 and Fig. 8 the velocity profile and turbulent kinetic energy respectively of pre-injection fluid have been compared for four

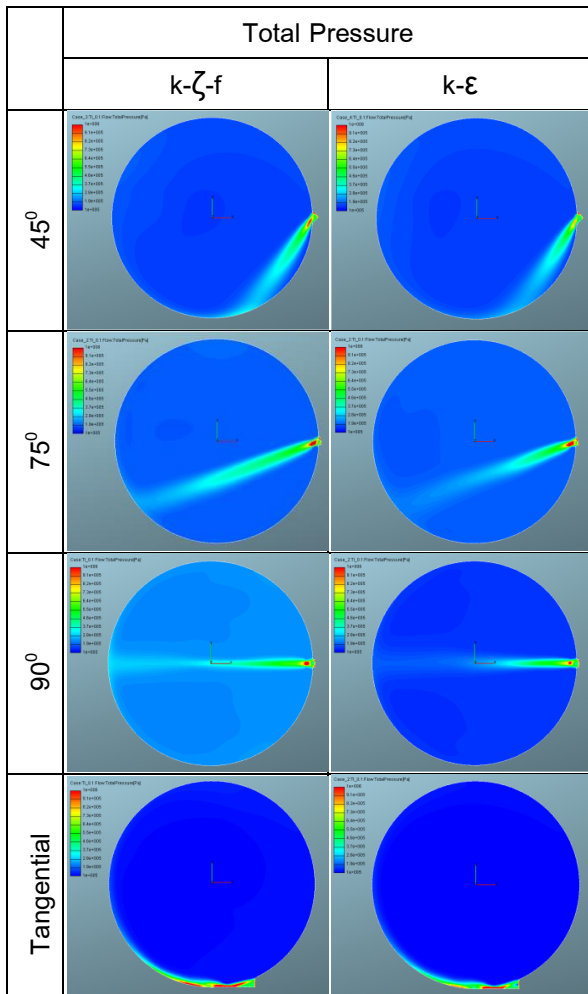


Fig. 6. Pressure distribution inside CVCC at time 0.1 s after the start of injection.

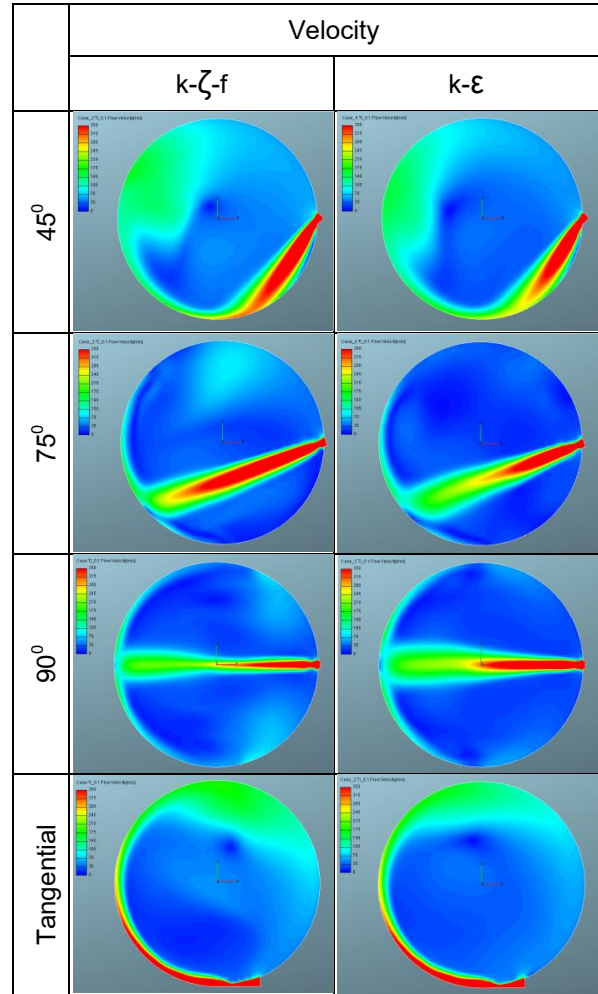


Fig. 7. Velocity Profile at time 0.1s after start of injection.

different angles of injection between two different turbulence models at time 0.1 seconds after the start of injection. In Fig. 7, it can be seen that the velocity is the highest at inlet because of higher pressure difference at the inlet than at other points. In Fig. 8, higher turbulent kinetic energy is observed in the direction of injection due to higher turbulence and fluctuation of velocity in the direction of injection.

There is not much difference visible in the results for pressure distribution, velocity profile and turbulent kinetic energy as observed from Figs. 6-8. So, the both the turbulence models are found to be in good agreement with each other for all the models with different injection angle.

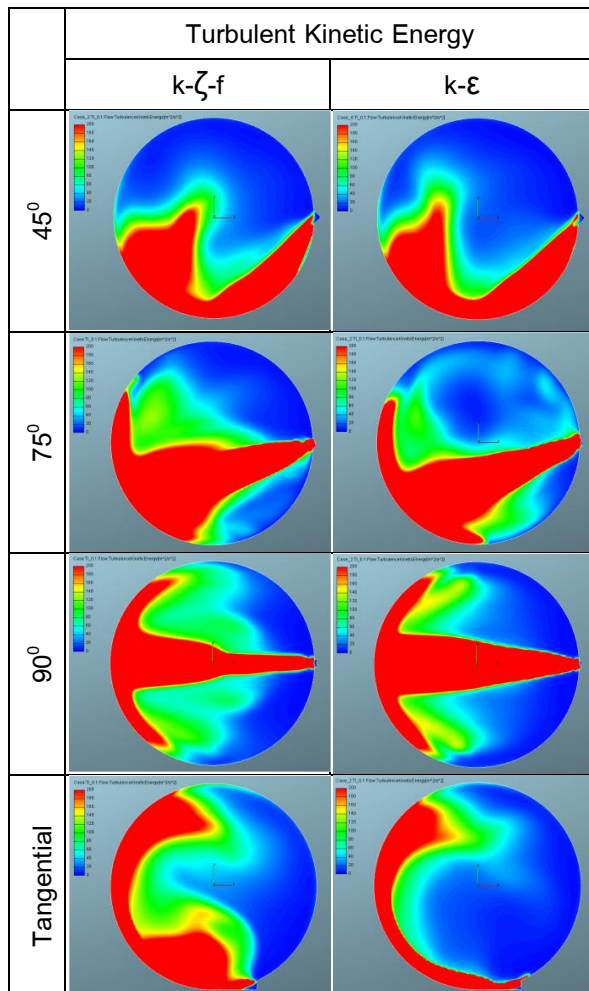


Fig. 8. Turbulent Kinetic Energy at time 0.1 s after the start of injection.

Since the results for the total pressure, in-cylinder flow velocity and turbulence kinetic energy for both the turbulence models are in good agreement, k- ζ -f model has been used for the simulation to calculate the total pressure, velocity and turbulence kinetic energy inside CVCC for different injection angle at different time i.e. at 0.1 s, 0.3 s, 0.5 s, 0.7 s, 0.9 s after the start of injection as shown in Figs. 9-11. In Fig.9, it can be observe that total pressure rises slower with time for the tangential inlet than other models due to high velocity at boundary as shown in Fig.10. So, the pre-injected gases inside CVCC with tangential

inlet have more time to mix and become a homogeneous mixture.

In Fig. 11, it can be observed that turbulent kinetic energy is higher at the center for the tangential inlet than other models with different injection angle at time after 0.5 s after the start of injection. Fig. 12 shows the mean average turbulence kinetic energy which is average of the values of turbulence kinetic energy shown in Fig. 11. As observed from Fig. 12 the value of turbulent kinetic energy inside CVCC for each of injection angle of 45^o, 75^o and 90^o is higher than that of the tangential inlet initially after the start of injection. However the value of turbulence kinetic energy for the tangential inlet is higher than that of other injection angle at time 0.4 s after the start of injection, which suggests that the gaseous mixture inside the CVCC with tangential inlet is more homogeneous. So, it is expected that CVCC model with tangential inlet is better than other models.

6. Conclusions

The following conclusions can be drawn from the present work:

1. The results in terms of pressure distribution, velocity profile and turbulent kinetic energy for the two turbulence models i.e. k- ζ -f and k- ϵ are in good agreement with each other for each model with all of injection angle.
2. The CVCC with tangential pre-injection inlet has higher turbulent kinetic energy at the centre and so it is expected that the pre-injected gases inside CVCC with tangential inlet form a better and homogeneous mixture than other injection angle.

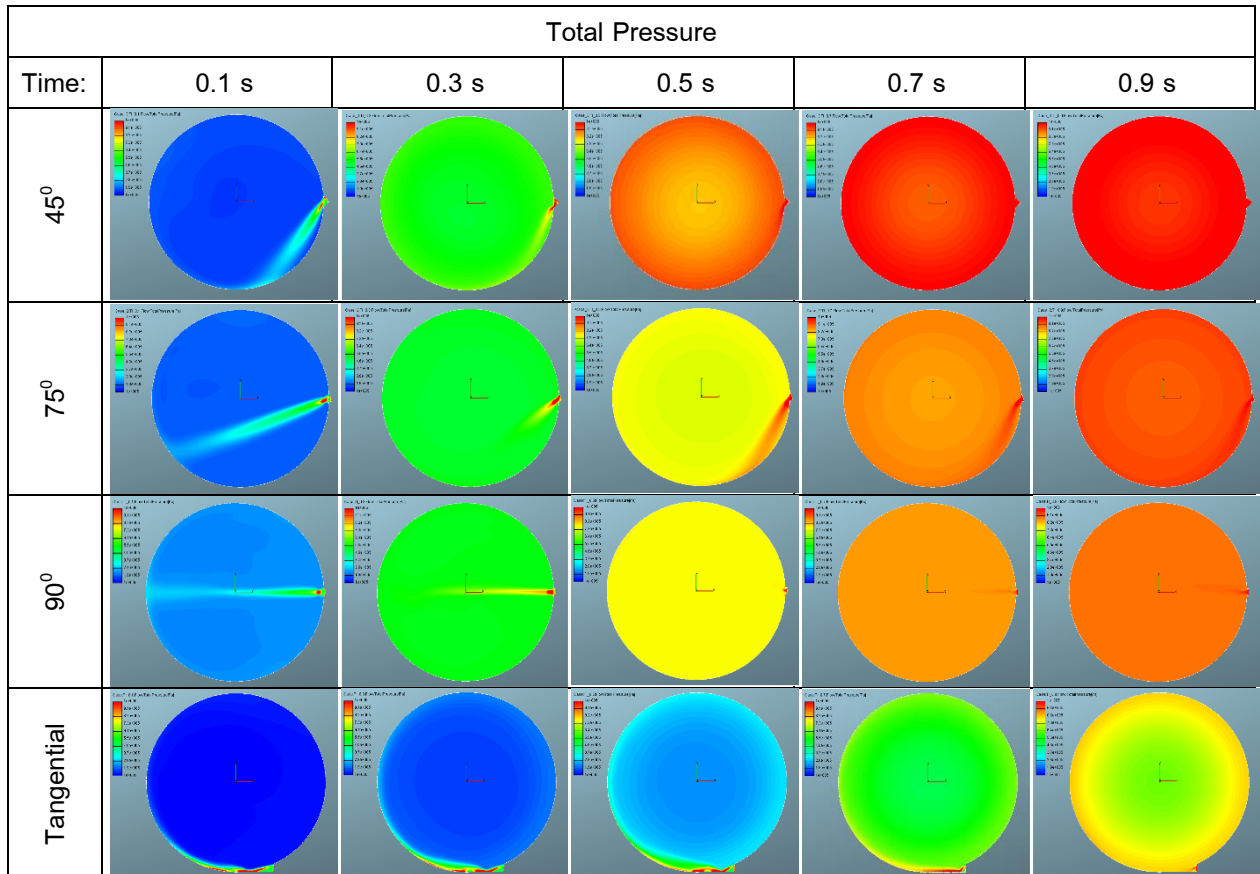


Fig. 9. Total Pressure inside CVCC with different injection angle at 0.1 s to 0.9 s after start of injection.

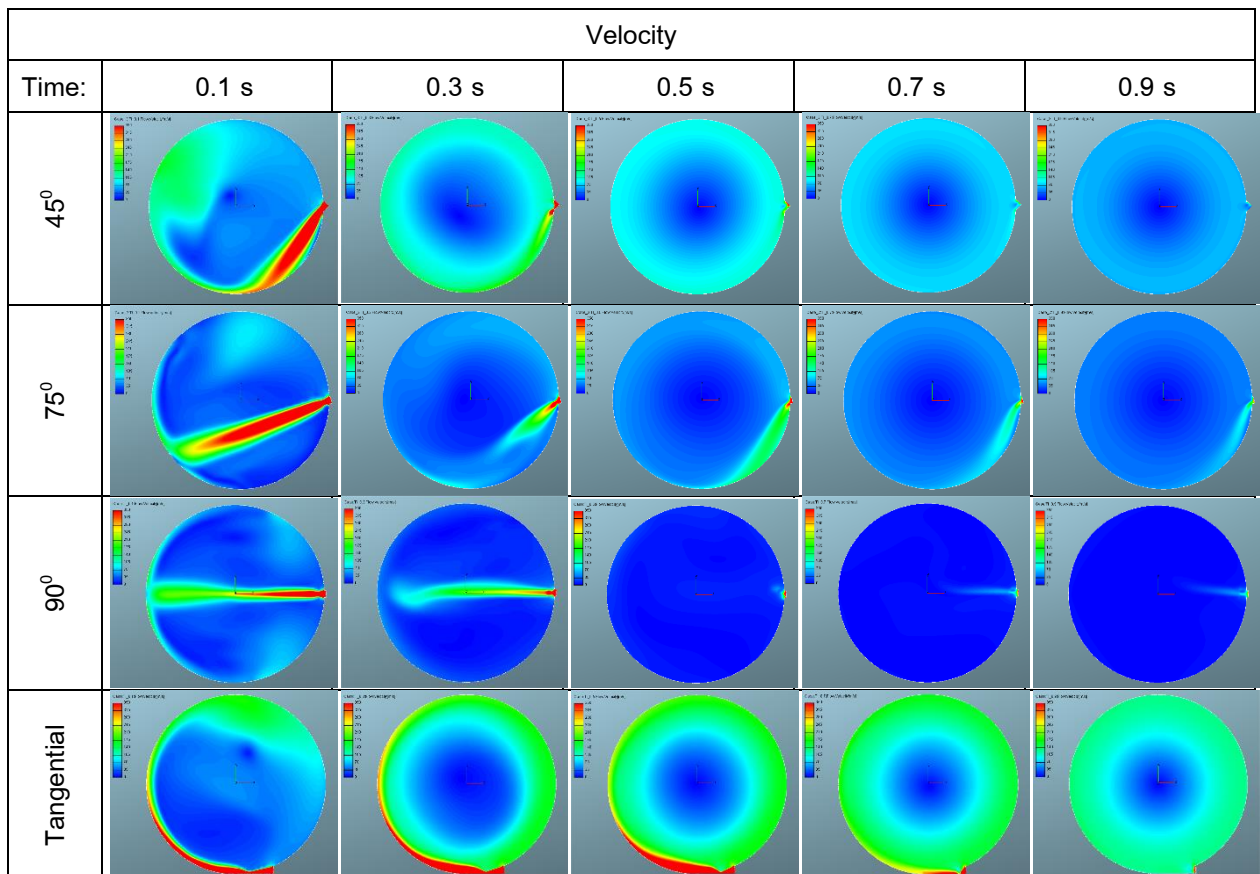


Fig. 10. Velocity profile inside CVCC with different injection angle at 0.1 s to 0.9 s after start of injection.

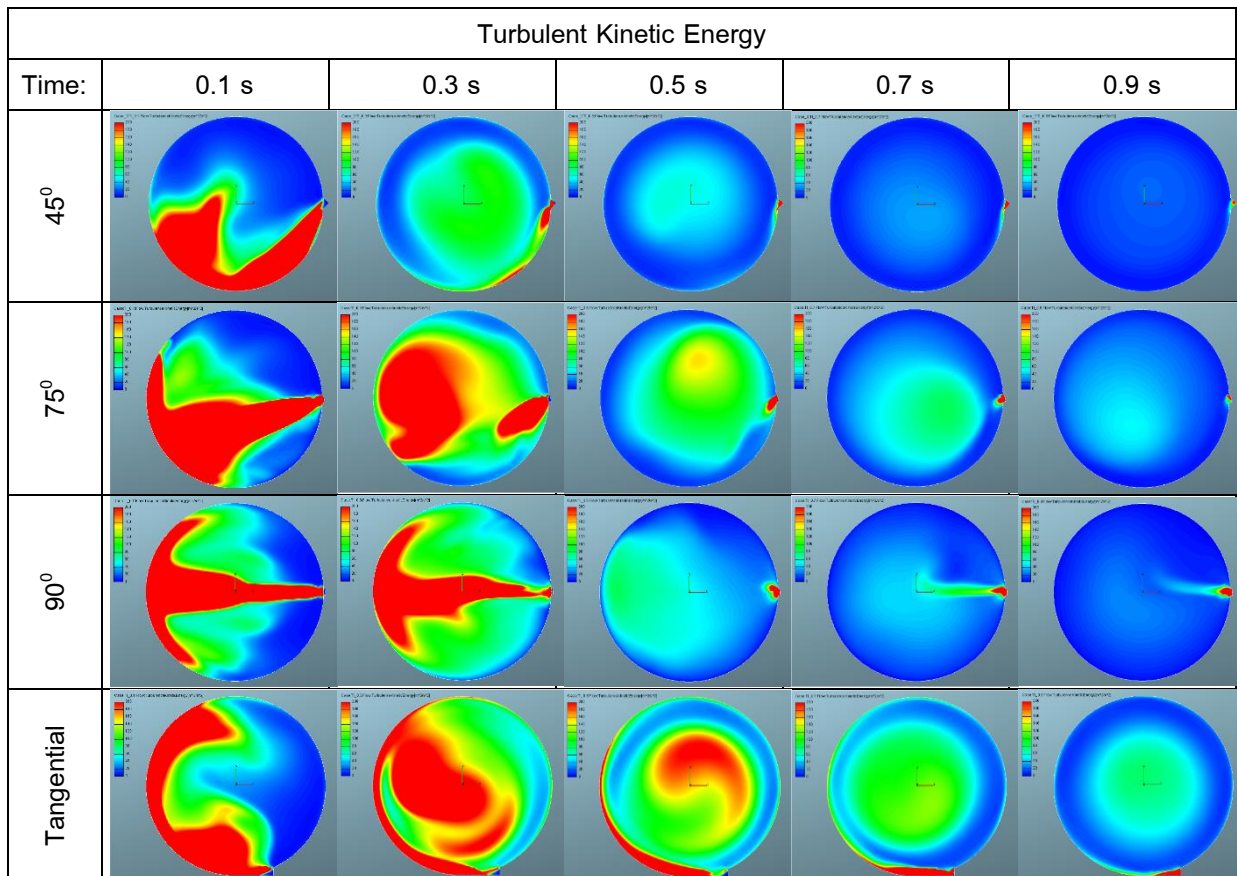


Fig. 11. Turbulent Kinetic Energy for different injection angle at 0.1 s to 0.9 s after start of injection.

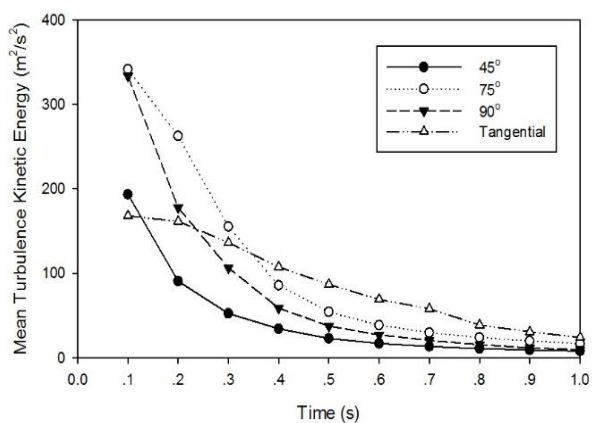


Fig. 12. Mean average turbulence kinetic energy for models with different injection angle.

7. Acknowledgement

The author gratefully acknowledges the support from Dr. Wishsanurak Wechsator, Dr. Arpiruk Hokpunna, Dr. Amornrat Kaewpradap as well as the company AVL for providing education licensed version of AVL FIRE[®] through the University Partnership Program.

8. References

- [1] Avinash Kumar Agarwal, Vipul H. Chaudhury (2012). Spray characteristics of biodiesel/blends in a high pressure constant volume spray chamber. *Exp Thermal and Fluid Sci* 2012; 42:212–218.
- [2] Baert, R., Frijters, P., Somers, B., Luijten, C. (2009). et al. Design and operation of a high pressure, high temperature cell for HD diesel spray diagnostics: guidelines and results, *SAE Technical Paper* 2009; 01-0649.
- [3] Oren, D., Wahiduzzaman, S., and Ferguson, C. (1984). A diesel combustion bomb: proof of concept. *SAE Technical Paper* 1984; 841358.
- [4] S.A. Basha, K.R. Gopal (2009), In-cylinder fluid flow, turbulence and spray models-A review, *Ren. Sust. Energy Rev.* 2009; 13: 1620–1627.

AEC035

[5] R. Hadeif, B. Lenze (2008), Effects of co- and counter-swirl on the droplet characteristics in a spray flame. Chem Engineering and Proc 2008; 47: 2209–2217.

[6] S.V. Patankar (1980), Numerical Heat Transfer and Fluid Flow. Hemisphere, New York, 1980.

[7] AVL Fire[®] (2011), CFD Solver Manual.

[8] K. Hanjalic, M. Popovac, and M. Hadziabdic (2004). A robust near-wall elliptic relaxation eddy viscosity turbulence model for CFD. International Journal of Heat and Fluid Flow, vol. 25, pp. 2004; 1047–1051.

[9] P. Durbin (1991). Near-wall turbulence closure modelling without damping functions. Theoretical and Computational Fluid Dynamics, vol. 3, pp. 1–13, 1991.

Appendix

A. Governing Equations

The mass conservation equation can be written as shown in Eq. (1).

$$\frac{\partial \rho}{\partial t} + \nabla(\rho U) = 0 \quad (\text{A.1})$$

Momentum equation in three directions x, y and z can be written as:

$$\frac{\partial(\rho U)}{\partial t} + \nabla(\rho U \times U) = -\nabla p + \nabla \tau + S_M \quad (\text{A.2})$$

where, ρ is the fluid density and U is three dimensional flow velocity in the x, y and z directions and p , τ and S_M are the fluid pressure, strain rate and momentum source, respectively.

B. Standard k- ϵ Model

The standard k- ϵ is a classical model which is based on transport equations for the turbulence kinetic energy (k) and its dissipation rate (ϵ):

$$\rho \frac{\partial k}{\partial t} + \rho U_j \frac{\partial k}{\partial x_j} = P + G - \epsilon + \frac{\partial}{\partial x_j} \left(\mu + \frac{\mu_t}{\sigma_k} \frac{\partial k}{\partial x_j} \right) \quad (\text{A.3})$$

$$\rho \frac{D\epsilon}{Dt} = \left(C_{\epsilon 1} + C_{\epsilon 3} G + C_{\epsilon 4} k \frac{\partial U_k}{\partial x_k} - C_{\epsilon 2} \epsilon \right) \frac{\epsilon}{k} + \frac{\partial}{\partial x_j} \left(\frac{\mu_t}{\sigma_\epsilon} \frac{\partial \epsilon}{\partial x_j} \right) \quad (\text{A.4})$$

where,

$$P = 2\mu_t S - (2/3)[\mu_t(\text{tr}S) + k](\text{tr}S) \quad (\text{A.5})$$

$$G = - \frac{\mu_t}{\rho \sigma_p} \nabla \rho \quad (\text{A.6})$$

Calculation of turbulent viscosity μ_t according to Prandtl–Kolmogorov [7] relation is given as

$$\mu_t = \rho C_\mu \frac{k^2}{\epsilon} \quad (\text{A.7})$$

and the coefficients have the following standard values as shown in Table 1.

Table.1 Value of constants in k- ϵ Model

C_μ	$C_{\epsilon 1}$	$C_{\epsilon 2}$	$C_{\epsilon 3}$	$C_{\epsilon 4}$	σ_k	σ_ϵ	σ_p
0.09	1.44	1.92	0.8	-0.373	1	1.3	0.9

C. The k- ζ -f Model

This model was developed by Hanjalic, Popovac and Hadziabdic [8]. This model is based on Durbin's elliptic relaxation concept, which solves a transport equation for the velocity scales ratio $\zeta = v^2/k$ instead of the equation for v^2 . The v^2 is the velocity scale and k is the turbulence kinetic energy. Durbin's model is described in [9]. The authors claim that due to a more convenient formulation of the equation for elliptic function f and especially of the wall boundary condition for this function, it is more robust and less sensitive to non-uniformities and clustering of the computational grid than Durbin's model [8]. Therefore, this model has been used here in AVL Fire code.

AEC035

The eddy-viscosity is obtained from

$$\mu_t = C_\mu \zeta \frac{k^2}{\varepsilon} \quad (\text{A.8})$$

and the rest of variables from the following set of model equation, thus

$$\rho \frac{Dk}{Dt} = \rho(P_k - \varepsilon) + \frac{\partial}{\partial x_j} \left[\left(\mu + \frac{\mu_t}{\sigma_k} \right) \frac{\partial k}{\partial x_j} \right] \quad (\text{A.9})$$

$$\rho \frac{D\varepsilon}{Dt} = \rho \frac{C_{\varepsilon 1}^* P_k - C_{\varepsilon 2} \varepsilon}{T} + \frac{\partial}{\partial x_j} \left[\left(\mu + \frac{\mu_t}{\sigma_\varepsilon} \right) \frac{\partial \varepsilon}{\partial x_j} \right] \quad (\text{A.10})$$

$$\rho \frac{D\zeta}{Dt} = \rho f - \rho \frac{\zeta}{k} P_k + \frac{\partial}{\partial x_j} \left[\left(\mu + \frac{\mu_t}{\sigma_\zeta} \right) \frac{\partial \zeta}{\partial x_j} \right] \quad (\text{A.11})$$

where, the following form of the f equations as adopted

$$f = L^2 \frac{\partial^2 f}{\partial x_j \partial x_j} = \left(C_1 + C_2 \frac{P_k}{\zeta} \right) \frac{(2/3 - \zeta)}{T} \quad (\text{A.12})$$

and the turbulent time scale T and length scale L are given by

$$T = \max \left(\min \left(\frac{k}{\varepsilon}, \frac{a}{\sqrt{6C_\mu |S| \zeta}} \right), C_T \frac{v^{3/2}}{\varepsilon^{1/2}} \right) \quad (\text{A.13})$$

$$L = C_L \max \left(\min \left(\frac{k^{3/2}}{\varepsilon}, \frac{k^{1/2}}{\sqrt{6C_\mu |S| \zeta}} \right), C_\eta \frac{v^{3/4}}{\varepsilon^{1/4}} \right) \quad (\text{A.14})$$

Additional modifications to the ε equation is that the constant $C_{\varepsilon 1}$ is dampened close to the wall, thus

$$C_{\varepsilon 1}^* = C_{\varepsilon 1} (1 + 0.045 \sqrt{1/\zeta}) \quad (\text{A.15})$$